Ozonolysis of Mixed Oleic Acid/*n*-Docosane Particles: The Roles of Phase, Morphology, and Metastable States

John D. Hearn and Geoffrey D. Smith*

Department of Chemistry, The University of Georgia, Athens, Georgia 30602

Received: July 16, 2007; In Final Form: August 22, 2007

The reaction kinetics of ozone with oleic acid (OA) in submicron particles containing *n*-docosane has been studied using aerosol CIMS (chemical ionization mass spectrometry) to monitor changes in particle composition. Internally mixed particles with $X_{OA} > 0.72$ were found to exist as supercooled droplets when cooled to room temperature. Partial reaction of the oleic acid was seen to completely inhibit further reaction and was attributed to the formation of a metastable solid rotator phase of the *n*-docosane at the surface. This reaction-induced phase change is believed to prevent further reaction by slowing ozone diffusion into the particle. When these particles were cooled to 0 °C before reaction, they reacted to a further extent and did not demonstrate such an inhibition. This shift in reactivity upon cooling is attributed to the formation of the thermodynamically stable form of *n*-docosane, the triclinic solid. This transition was accompanied by an increase in the *n*-docosane density, which led to the development of "cracks" through which ozone can diffuse into the particle. The aerosol with $X_{OA} < 0.72$ consisted of an external mixture of particles containing *n*-docosane in either the rotator or the triclinic solid phase because of the stochastic nature of the rotator → triclinic transition. The reactivity of the oleic acid was seen to increase with increasing *n*-docosane content as a larger fraction of the particles underwent the rotator → triclinic transition and therefore contained cracks at the surface. These findings demonstrate the importance of transient, metastable phases in determining particle morphology and how such morphological changes can influence rates of reactions in organic aerosols.

Introduction

Although simple in molecular composition, normal alkanes, $CH_3-(CH_2)_{n-2}-CH_3$ (C*n*), are known to exhibit a variety of interesting behaviors and have been studied extensively for several decades. An excellent review of the properties of *n*-alkanes is given by Small.[1] These long-chain, aliphatic molecules also serve as a starting point for understanding the behavior of many derivative molecules because they are the building blocks of lipids, surfactants, polymers, and liquid crystals. Of particular interest is the rich phase behavior of the *n*-alkanes, which can form crystal structures of triclinic, monoclinic, or orthorhombic symmetry.[1] In addition, they can exist in five plastic-crystalline phases, also called "rotator" phases, between the fully ordered crystalline phases and the isotropic liquid phase.[2] These rotator phases exhibit long-range positional order in three dimensions but no long-range order with respect to rotation about the molecule's long axis.[2,3] The rotator phases are less dense than the crystalline phases and have very large coefficients of thermal expansion, isothermal compressibility, and heat capacity.[2]

Many of the interesting properties of *n*-alkanes can be attributed to or are influenced by these rotator phases,[4,5] including the well-known odd−even effect in their melting points and crystal structures and the amount by which they can be supercooled, i.e., the difference between the equilibrium transition temperature and the temperature at which the transition actually occurs when cooled.[6,7] In addition, it has been demonstrated that *n*-alkanes form an ordered surface frozen monolayer of the rotator phase that is in equilibrium with the disordered liquid a few degrees Celsius above the melting point.[8−10] Frozen surface layers have been found to exist for *n*-alkanes with $14 < n \leq 50$ using a variety of techniques, including surface tension measurements,[8,11] X-ray scattering,[9,12] light scattering,[13] and differential scanning calorimetry.[14] The existence of the frozen surface layer has been attributed to the thermodynamic favorability of replacing the liquid−vapor interface with the solid−vapor and solid−liquid interfaces;[15] in other words, the free energy is lowered upon formation of the frozen monolayer. This surface frozen layer has been shown to mediate bulk crystallization and has been hypothesized to act as a nucleation site.[16−18] Even if it exists only as a transient, metastable phase, the rotator can determine the growth morphology of the crystalline solid.[5] Thus, a complete description of the phase behavior of melts containing alkanes or their derivatives requires an understanding of the roles that the rotator phases play.

Despite the wealth of information regarding the phase behavior of *n*-alkanes, only a few studies have been performed on mixtures containing *n*-alkanes and other molecules, such as alcohols,[19] ketones,[20] or surfactants.[21] What is more, no experiments to study the effects of alkane-mediated morphology changes on reactions in such mixtures have been reported. Such effects could be of significant interest for the refining of petroleum given that the crystallization of waxes from crude oils (containing aliphatic hydrocarbons) can cause a variety of problems.[22−24] Furthermore, the reactions of organic aerosol particles in the atmosphere could be influenced greatly by the phase and/or morphology as determined by *n*-alkanes and their derivatives. Aerosols in the troposphere are known to contain a significant fraction of organic material accounting for 20−40% of the fine particulate mass in rural areas in the U.S. and 30−80% in urban areas.[25] This material consists of many different classes of organic molecules including *n*-alkanes that are known to originate from the disintegration of plant material[26] and the combustion of diesel fuel.[27,28]

* To whom correspondence should be addressed. E-mail: gsmith@chem.uga.edu.

10.1021/jp0755701 CCC: $37.00
Published on Web 10/05/2007

Here, we examine how the phases and morphologies of aerosol particles are influenced by a particular *n*-alkane, *n*-docosane (C22), $CH_3-(CH_2)_{20}-CH_3$, and how this determines the rate of a "probe" reaction in the particle. The probe reaction employed is that of gas-phase O_3 with an unsaturated fatty acid, oleic acid (OA), in mixed OA/C22 particles. This reaction was chosen, in particular, because it has been studied extensively in the atmospheric chemistry community as a model for understanding the oxidation of organic aerosols.[29−39] Because C22 does not react with O_3, any changes in OA reactivity can be attributed to changes in the phase and/or morphology of the particles associated with the *n*-alkane. A few recent studies have already found that OA reactivity can be reduced by more than an order of magnitude in mixtures containing solid saturated fatty acids,[40−44] so there is reason to believe that this solid *n*-alkane might have a similar effect.

By monitoring the changes in aerosol particles on-line as they react in a flow tube, we are able to study the behavior of this system free from the constraints accompanying bulk samples in which contact with substrate surfaces can initiate heterogeneous nucleation. Furthermore, the small sample volume of the submicron particles significantly lowers the rate of nucleation as compared to bulk or even electrodynamic balance studies, which typically employ particles 30 μm or larger.[18] Thus, it is possible to observe the effects of metastable phases in these aerosol experiments that might otherwise be difficult to study. In particular, we find that the reactivity of OA is influenced by the presence of C22 and that the magnitude of this effect depends on whether C22 exists in a metastable rotator phase or in the triclinic crystalline phase. Furthermore, the reaction between O_3 and OA is seen to induce the formation of the rotator phase in some particles, leading to a dramatic decrease in OA reactivity.

Experimental Methods

Mixed particles containing OA and C22 were generated using homogeneous nucleation, as previously described.[44] With this method small flows of N_2 (100 sccm) were sent through heated reservoirs containing OA (140−160 °C) and C22 (80−190 °C), and the saturated vapors were mixed and heated again (400 °C). The mixed flow cooled to room temperature, forming internally mixed particles. Particles of 700-nm diameter (geometric standard deviation ≤ 1.15) were then selected from the polydisperse aerosol using an electrostatic classifier (model 3080, TSI, Inc.). The sheath flow of the classifier was sent through a dry ice/isopropanol bath (−70 °C) to remove ammonia, apparently originating from the internal tubing of the electrostatic classifier, which interfered with the chemical ionization in the aerosol CIMS. Particle concentration was not routinely measured but was approximately 1−10 $\mu g/m^3$ in the flow tube. For the "precooling" experiments, the aerosol was passed through a glass trap immersed in a cold water bath of variable temperature (0−15 °C) before entering the flow tube. The residence time in the trap was sufficiently long (i.e., several seconds) to ensure that the particles reached thermal equilibrium. Likewise, the particles re-equilibrated to room temperature after leaving the trap and before entering the flow tube.

The mixed particles reacted with O_3 at atmospheric pressure and room temperature (23 ± 2 °C) in an aerosol flow tube as has been described elsewhere.[38] Briefly, the particles were introduced through a moveable glass injector tube ($^1/_4$-in. o.d.) that allowed the reaction time to be varied (0−5 s) depending on its position. The particle transit times in the flow tube were measured as described previously.[33] The particles were entrained in the carrier gas flow (1.5 slpm) and remained on axis, minimizing losses to the flow tube walls. O_3 was created from O_2 using a corona-discharge generator (Pacific Ozone Technology, Inc.) and stored on a silica gel trap held in an isopropanol/dry ice bath (−70 °C);[33] it was swept out of the trap using a N_2 flow (20−50 sccm) that mixed with a larger flow of N_2 (500 sccm) that carried it into the rear of the flow tube. The O_3 concentration was measured before entering the flow tube using a 10-cm-long absorption cell with a Hg lamp (UVP, 11SC-1) and a UV-sensitive photodiode (Newport, 818-UV). Typical O_3 concentrations in the flow tube were $(2-3) \times 10^{15}$ molecules/cm^3.

Upon exiting the flow tube, the particles were sampled into the aerosol CIMS instrument through a heated glass capillary inlet held at approximately 350 °C. The vapor from the heated particles was then chemically ionized with NO^+, which was generated by sending a small flow (0.5 sccm) of NO through the ^{210}Po ionizer (NRD, Inc.). The NO^+ reagent ion was used because it is capable of ionizing both OA and C22 through hydride abstraction, yielding the $[OA - H]^+$ ($m/z = 281$) and $[C22 - H]^+$ ($m/z = 309$) ions, respectively. Additionally, some of the OA (∼20−30%) appears as the NO^+ adduct, $[OA + NO]^+$, although it was not used in these experiments. The OA/C22 content in the particles was determined from the relative integrated peak intensities in the mass spectra. Daily calibrations of OA and C22 were performed using an aerosol with a known OA and C22 composition.

The phase diagram for the binary system was constructed using a differential scanning calorimeter (DSC) (Perkin-Elmer, model DSC 7). Mixtures of known composition ranging from $X_{OA} = 0.12$ to $X_{OA} = 0.92$ were used as well as pure OA and pure C22, and an empty aluminum pan was used as the reference. The mass of each sample was not measured, but it was approximately 50 mg. The heat flow into or out of the sample was measured as the sample was heated or cooled at a constant temperature ramp rate of ±5 °C/min, and the temperature at the peak of the melting transition was taken as the melting point. A few experiments were performed in which the temperature was varied by 2 °C/min to more precisely resolve certain phase transitions.

Gases were purchased from National Welders Supply with the following purities: N_2, 99.99%; O_2, 99.99%; and NO, 99.5%. Oleic acid (99%) was purchased from Sigma-Aldrich, and *n*-docosane (98%) was purchased from Fluka.

Results

DSC Experiments. The starting point for understanding the behavior of the mixed OA/C22 particles is the equilibrium phase diagram of bulk OA/C22 mixtures. The phase diagram was constructed from the OA and C22 melting transitions observed in the DSC experiments for a variety of compositions (Figure 1). An example DSC trace of a mixture with $X_{OA} = 0.31$ is shown in Figure 2. In this experiment, the temperature was raised and lowered at 2 °C/min, whereas in most of the others, the temperature ramp was ±5 °C/min.

The heating trace contains two positive-going peaks, one representing the melting of OA (at 11.0 °C) and one representing the melting of C22 (at 43.4 °C), the triclinic (T) → liquid (L) transition. In the cooling trace, the OA freezes at 4.2 °C, nearly 7 °C below the melting point. This difference results from the supercooling of the OA as the temperature is lowered below its melting point. This phenomenon is not uncommon even in bulk measurements such as those made here, and in fact, OA has been observed to be supercooled by up to 8 °C on the walls of a glass flow tube.[37]

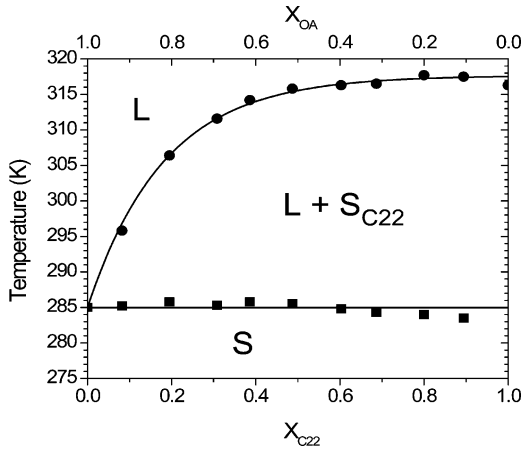

Figure 1. Phase diagram of bulk oleic acid (OA)/*n*-docosane (C22) mixtures determined from the melting transitions of oleic acid (■) and *n*-docosane (●) using differential scanning calorimetry. L, liquid mixture; L + S_{C22}, liquid mixture and solid *n*-docosane; S, solid oleic acid and solid *n*-docosane.

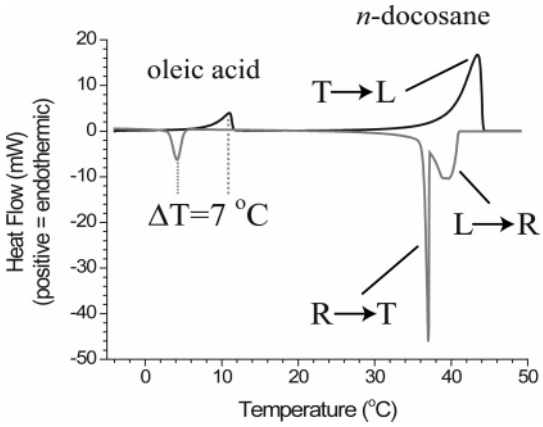

Figure 2. Differential scanning calorimetry trace of a mixture with $X_{OA} = 0.31$ heated (black line) or cooled (gray line) at a constant rate of 2 °C/min. Oleic acid is observed to be supercooled by 7 °C (ΔT). The existence of *n*-docosane in the metastable R phase leads to a separation of the L → R and R → T transitions upon cooling.

Similar supercooling is also evident for C22, although the single triclinic (T) → liquid (L) transition has separated into two phase transitions: (1) At 39.0 °C, the liquid (L) → rotator (R) transition occurs, and 2) at 37.0 °C, the rotator (R) → triclinic (T) transition occurs. The split happens because the C22 exists as a supercooled liquid between 43.4 and 39.0 °C and then as a metastable R solid between 39.0 and 37.0 °C. The sum of the areas under these two peaks equals the area under the single T → L melting peak, as expected. Such supercooling of the liquid and the rotator phases has been observed previously for bulk *n*-alkanes including *n*-docosane[5,45,46] and is represented graphically in the plot of Gibbs free energy vs temperature in Figure 3. The mixed aerosol particles employed in the flow tube studies (below) are expected to show similar behavior, although they should exist in the supercooled liquid and metastable rotator phases over even wider temperature ranges; the rates of nucleation in the particles will be even lower than in the bulk because they are not in contact with surfaces and contain significantly smaller sample volumes.

We would like to point out that, although we have considered the R solid as one specific phase, in fact, for pure C22, it really represents two different metastable rotator phases, R_I and R_{II}. The L → R_{II} transition occurs first followed by the R_{II} → R_I transition at a lower temperature.[3] This R_{II} → R_I transition involves a distortion of the hexagonal packing and is accompanied by a small enthalpy change of 1.0 kJ/mol[47] (compared to 49.0 kJ/mol for the melting transition[1]); consequently, it is not distinguishable in the DSC traces. Although these two rotator phases exhibit different degrees of symmetry, neither contains long-range order in the rotational degree of freedom. Each R solid contains gauche bonds that introduce bends and kinks into the aliphatic chains, distinguishing them from the T phase in which the chain adopts an all-trans configuration. This difference results in a larger density for the T phase than for either of the R phases,[1] and because this distinction is important for understanding the phase behavior of C22 in the mixed OA/C22 particles, we consider the R_I and R_{II} phases as one metastable R phase in this study.

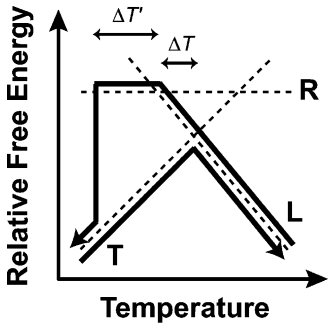

Figure 3. Free energy schematic (after Figure 3a of Sirota[16]) illustrating the existence of supercooled liquid *n*-docosane (ΔT) and the metastable R phase of *n*-docosane ($\Delta T'$) upon cooling.

Flow Tube Experiments. The reactivity of OA with O_3 in mixed OA/C22 particles was studied in an aerosol flow tube with a moveable particle injector allowing the reaction time to be varied (0−5 s). For each particle composition, the OA content was measured using aerosol CIMS as a function of reaction time in order to construct an OA decay curve (Figure 4a,b). As expected, the C22 signal (not shown) was not observed to decay from reaction, but it did fluctuate, presumably from variations in the particle concentration. Consequently, the OA signal was normalized to the C22 signal in order to account for these variations. Trends in the initial rate of reaction (Figure 5a) and the amount of OA remaining at the end of the decay (Figure 5b) were observed depending on the initial particle composition. In particular, the particles exhibit two different types of behavior depending on whether the particles are "OA-rich" (region I, $X_{OA} > 0.72$) or not (region II, $X_{OA} < 0.72$).

In region I, the initial rate of OA reaction is high (i.e., similar to the rate of pure OA particles), and the OA reaction stops abruptly before all of the OA reacts. This sudden shift in reactivity indicates that a fraction of the OA is prevented from reacting with O_3, or is "trapped". Furthermore, this fraction must not be trapped before reaction; otherwise, the initial rate of reaction would be correspondingly lower. Put another way, if the trapped OA were present before reaction, it would "dilute" the untrapped OA so that the observed initial rate of reaction (i.e., the initial slope in Figure 4a), would be lower. Thus, we can conclude that the reaction between OA and O_3 induces a change in the particles that prevents further reaction. We believe that this change results from a C22 phase transition (L → R) that leads to a sudden change in particle morphology. The issues of how this transition occurs and what kind of morphology is adopted are addressed in the Discussion below.

In region II, the rate of reaction is low initially but increases in the particles that contain more C22; conversely, the amount of OA trapped decreases. We conclude that, unlike in region I, some of the OA is trapped before reaction and this amount decreases in particles with more C22. The initial reactivity is also decreased proportionally to the amount that is trapped. We believe that these observations can be attributed to the existence of C22 in two different solid phases, R and T, with the

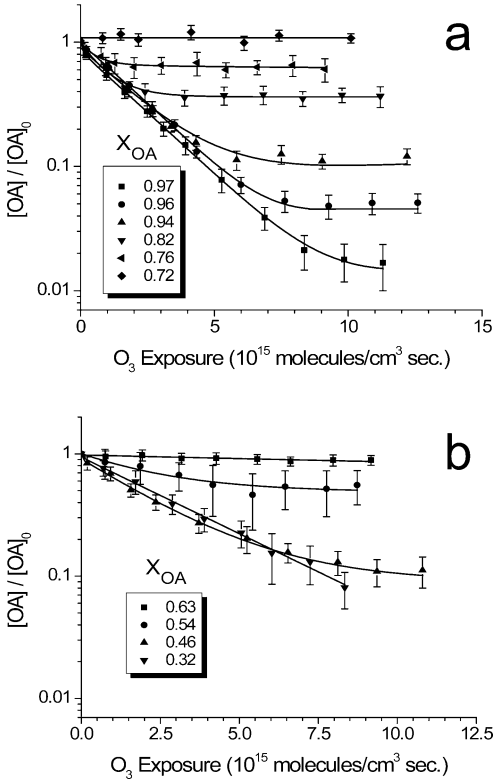

Figure 4. Oleic acid (OA) reaction decay curves for mixed oleic acid/*n*-docosane aerosols with (a) $X_{OA} \geq 0.72$, for which the O_3 + OA reaction induces the L → R transition for *n*-docosane, leading to trapping of the remaining oleic acid (plateau in decays), and (b) $X_{OA} < 0.72$, which consists of an external mixture of particles containing *n*-docosane in either the R or T solid phases with the proportions determined by the *n*-docosane content. Error bars represent 1σ in the measured OA signals. Lines are to guide the eye.

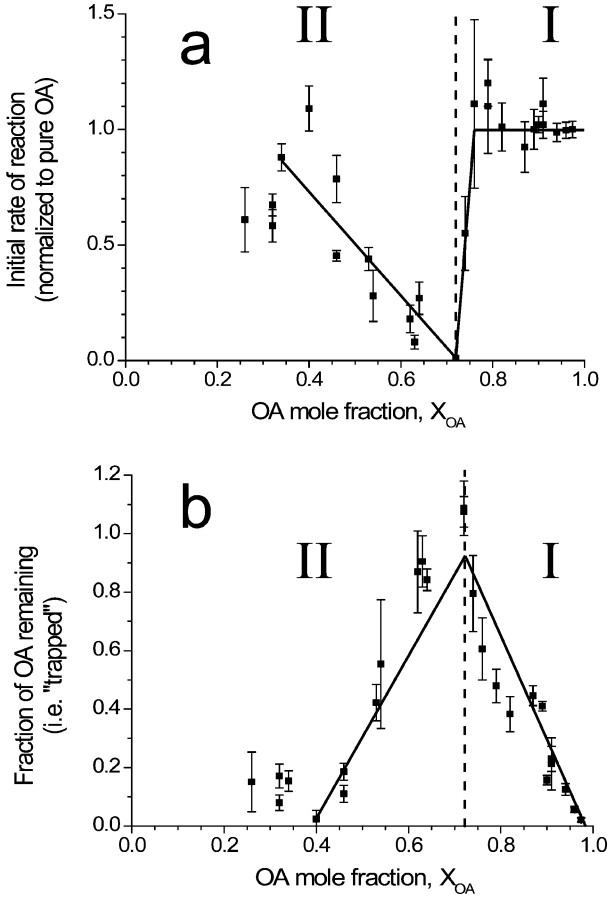

Figure 5. (a) Initial rate of reaction and (b) fraction of oleic acid (OA) remaining as determined from the oleic acid reaction decay curves for particles of varying composition. Particles can be grouped according to trends in reactivity, which indicate the initial phase of the *n*-docosane as a liquid (region I) or a liquid/solid mixture (region II). Note that, for $X_{OA} < 0.40$, the oleic acid did not react to completion over the time scale of the experiments, so the amount remaining plotted in b is an upper limit to the amount trapped. Error bars were determined from the standard deviation of the measured OA signals. Lines are to guide the eye and do not represent fits to the data.

distribution of these phases determined by the strong dependence of the rate of the R → T transition on the C22 content.

Discussion

We can now develop a picture of how the mixed OA/C22 particles form and how their morphologies influence the rate of the OA + O_3 reaction. Because all of the reactions are carried out at 23 (±2) °C, well above the OA melting point of 12 °C, the OA exists in the liquid phase. At equilibrium, the phase diagram (see Figure 1) indicates that C22 exists as a liquid for $X_{OA} \geq 0.92$ and as both a solid and a liquid for $X_{OA} < 0.92$. However, because all particles are cooled from elevated temperature ($T \approx 400$ °C) to room temperature, it is possible for them to exist in supercooled or metastable phases. Consequently, the C22 exists as a liquid (L), a rotator solid (R), or a triclinic solid (T). The phase(s) in which the C22 exists is (are) determined by the temperature, the temperature history (i.e., rate of cooling or whether the particles are precooled before reaction), the composition of the particle, and the extent of reaction within the particle. The rate of the OA + O_3 reaction is strongly influenced by the phase of the C22, and the particles can be grouped into two regions depending on whether they are present initially as a liquid (region I, $X_{OA} > 0.72$) or as a liquid/solid mixture (region II, $X_{OA} \leq 0.72$). Below, we consider these two regions and examine how the phase of the C22 in the particles affects the observed reactivity of the OA.

Region I ($X_{OA} > 0.72$). Particles are liquid droplets, and the rate of OA reaction is high (see Figure 5a) because O_3 can diffuse throughout the droplet. For $X_{OA} \geq 0.92$, such behavior is not unexpected because the phase diagram predicts that the particles will exist as a liquid. However, particles with $X_{OA} < 0.92$ also remain entirely liquid even as the temperature falls below the freezing point because they are supercooled. In other words, the rate of nucleation is not sufficient to induce solidification of the C22 on the time scale of these experiments (i.e., several seconds). There is substantial evidence for supercooling in *n*-alkanes, and indeed, we observed it to happen even in the DSC measurements of the bulk C22 and OA/C22 mixtures (e.g., Figure 2). The small volumes of the particles and the lack of contact with surfaces that could initiate nucleation make it possible for the particles to remain supercooled longer and over an even wider temperature range than is possible with bulk samples. Thus, the initial decay of OA is the same for all particles in region I (see Figure 5a) because they all begin as liquid droplets.

Reaction between O_3 and OA makes the particle no longer metastable as a liquid, and the L → R transition in the C22 is initiated. It is not clear how this transition occurs, but the reaction does change the composition of the particle substantially. Nonanal, in particular, is a semivolatile product, and its evaporation could remove enough energy near the surface to create a local temperature gradient. Although this evaporation is not fast enough to cool the entire particle, it could enhance the aggregation of C22 molecules forming "seeds" of bundled

segments of trans-planar chains. Such seeds have been found to initiate crystallization of alkanes[48] and could induce the formation of solid R in these particles. Additionally, increases in the local C22 concentration near the surface that might occur upon evaporation of the nonanal could speed up the nucleation. Once the nuclei are formed, the solid R forms a frozen surface layer that then acts as a heterogeneous nucleation site from which the bulk of the particle can form the R solid. There is substantial experimental[4,5,8,11,18,49,50] and theoretical[51−53] evidence for both the formation of and the nucleation by surface frozen layers in *n*-alkanes and mixed systems containing *n*-alkanes. Furthermore, the geometry and symmetry of the surface frozen layer have been found to closely resemble the R solid (specifically, the R_{II} rotator phase).[15,54] We believe that the frozen layer that is formed consists entirely of C22 in these mixed OA/C22 particles because of repulsion between the carboxylic acid moiety of OA and the alkyl chains of C22; a similar segregation has been observed in mixed *n*-alkane/*n*-alcohol systems and has been attributed to repulsion between the alcohol groups and the alkyl chains.[19] The R solid that forms in the particle is not the thermodynamically stable phase (which is T), but it can exist as a metastable phase in much the same way that the particle remains liquid when it is supercooled. In fact, the R → T transition in C22 is known to be supercooled by as much as 7 °C,[4,46] and we have observed such supercooling in our bulk DSC studies (e.g., Figure 2).

Once the surface frozen R layer has formed, the reaction between O_3 and OA is severely inhibited, as evidenced by the plateaus in the OA decays (Figure 4a). The O_3 solubility and/or diffusion into the particle is greatly reduced by the solid R layer that forms at the surface after being initiated by the O_3 + OA reaction. In essence, the remaining OA is trapped because O_3 can no longer penetrate the particle. The fractional amount of OA that is trapped increases with decreasing OA content in region I (see Figure 5b), because the particle is supercooled by a larger amount and less of a perturbation (i.e., reaction) is required to initiate the nucleation. Finally, at a composition of $X_{OA} = 0.72$, the particle can no longer remain a supercooled droplet at room temperature, and the C22 freezes out to the R phase even before OA reacts with O_3; consequently, all of the OA is trapped. From this observation and the bulk phase diagram (Figure 1), we determine that the OA/C22 particles can be supercooled by up to 14 °C.

Although this picture satisfactorily explains the observed trends in reactivity, why is it necessary that C22 exist in the R phase? Why is the thermodynamically stable T phase not formed (i.e., L → T), trapping the OA? If this were the case, then we would expect to observe the trapping when we induce the L → T transition by precooling the particles to 0 °C and then warming them back to room temperature before they enter the flow tube. On the contrary, such experiments (Figure 6a) show that not only do precooled particles react, they react to completion. Consequently, we conclude that the C22 exists in two different solid phases (R or T) depending on whether the particles are precooled or not. Furthermore, these phases demonstrate markedly different trapping properties.

So, why then does the R phase trap OA whereas the T phase does not? Both phases are highly ordered and tightly packed solids with an average area per molecule of only approximately 20 Å^2.[17] The distance between adjacent molecules is then only on the order of 4−5 Å, which is similar to the size of the O_3 molecule. For example, Vieceli et al. represented O_3 as a sphere with a diameter of 4 Å in their molecular dynamics study of its interaction with various long-chain molecules.[55] It is then

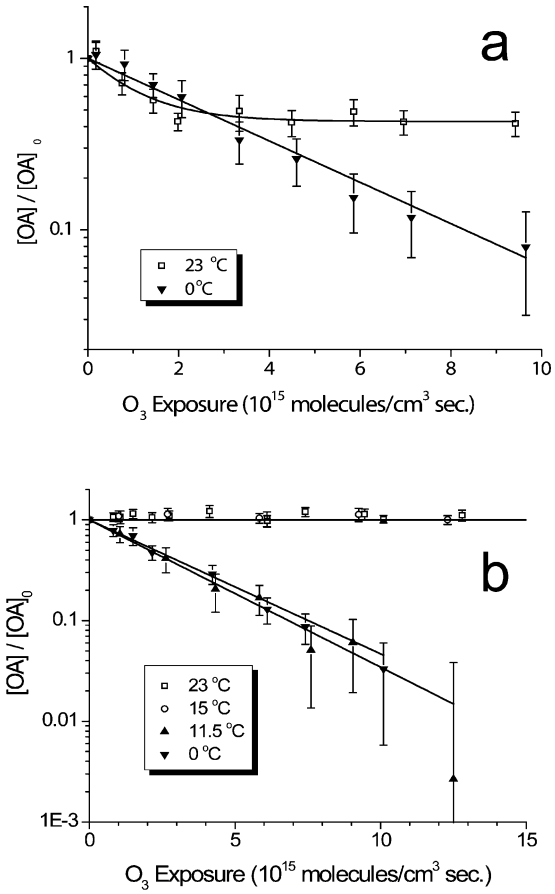

Figure 6. Oleic acid (OA) reaction decay curves for precooled mixed oleic acid/*n*-docosane particles with (a) $X_{OA} = 0.87$ and (b) $X_{OA} = 0.72$. Particles were brought to the desired temperature (□, 23 °C; ◇, 15 °C; ▲, 11.5 °C; ▼, 0 °C) and then allowed to warm to 23 °C before reacting. Precooling is seen to enhance the oleic acid reactivity and is attributed to the R → T transition of the solid *n*-docosane upon cooling. Error bars represent 1σ in the measured OA signals. Lines are to guide the eye.

reasonable to expect that O_3 would not be able to intercalate either the solid R or T alkane layers at the surface of the particle. However, because some of the bonds in the R phase exist in the gauche configuration, bends and "kinks" are created in the alkyl chain,[56] and the density of the R phase is lower than that of the T phase; for example, the density of *n*-tetracosane, C24, increases from 0.86 g/cm^3 in the R phase to 0.92 g/cm^3 in the T phase.[57] Consequently, when the R → T transition occurs, the increase in density breaks the C22 crystal into blocks and creates "cracks" or "channels" through which the O_3 can reach the OA inside the particle and through which the OA can diffuse to the surface. In Figure 7, we illustrate how such a change in density can expose the OA to the O_3, although more dramatic changes in morphology might occur. For example, the blocks of C22 at the surface could be displaced by OA, in which case the particle would consist of domains of C22 surrounded by OA. Such a scenario could explain the dramatic increase observed in the OA reactivity, although we have no means by which to characterize the surface morphology. Nonetheless, reaction is observed when C22 is in the T phase because it does not form directly from the isotropic L phase but rather forms from the metastable solid R phase. Thus, the metastable R phase determines the morphology of the particle and, therefore, the reactivity of the OA within. We point out that the granular substructure formed in the crystallization of polymers has also been attributed to the formation of blocks and nucleation mediated by a metastable phase,[58] just as is the case here.

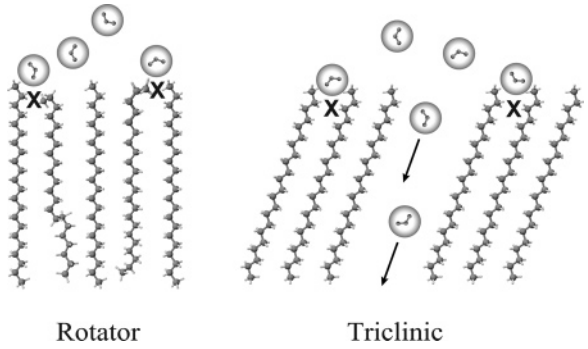

Figure 7. Schematic representation of the rotator (left) and triclinic (right) solid phases of *n*-docosane believed to be present at the surface of the mixed oleic acid/*n*-docosane particles. The increase in density accompanying the R → T transition leads to the formation of blocks of *n*-docosane (right), creating cracks through which O_3 can diffuse into the particle to react with oleic acid. The O_3 is represented by a sphere with a 4-Å diameter after Vieceli et al.[55]

This distinction also explains the marked increase in reactivity when particles with $X_{OA} = 0.72$ are sufficiently precooled (Figure 6b). No reaction is evident when the particles are at room temperature or even when they are precooled to 15 °C before entering the flow tube. However, when they are precooled to 11.5 or 0 °C, the OA is seen to react almost completely. We surmise that the particles undergo the R → T transition when precooled to 11.5 °C (or below), and as a result, cracks are formed, and the O_3 penetrates into the particle to react with the OA. At higher temperatures, the C22 remains in the R phase, and O_3 transport into the particle is impeded.

Region II ($X_{OA} < 0.72$). The aerosol consists of an external mixture of particles that contain solid C22 in either the R phase or the T phase, as well as liquid C22 and liquid OA. Those particles containing C22 in the R phase behave similarly to the $X_{OA} = 0.72$ particles; that is, no OA reaction occurs. Those particles containing C22 in the T phase behave similarly to the precooled $X_{OA} = 0.72$ particles in which the R → T transition was induced before reaction; that is, the OA reacts to completion. The observed OA decays reflect the average of these two cases weighted by the number of particles of each type. Thus, the initial rate of reaction of OA in these particles is seen to be lower than that in pure OA particles (Figures 4b and 5a), which can be attributed to the averaging of the OA decays from the R particles (i.e., no reaction) and the T particles (i.e., fast reaction). The particles that are richer in C22 are more likely to exist in the T phase because the R → T transition is faster; consequently, the initial rate is observed to increase and the amount of OA trapped is observed to decrease at lower X_{OA} (Figures 4b and 5b). Finally, at $X_{OA} = 0.40$, the C22 in the R phase is no longer stable at room temperature, and all of the particles contain C22 in the T phase. At this point, precooling of the particles has no effect on the observed OA decays (data not shown) because the C22 is already in the T phase.

How is it possible for particles of the same nominal composition (i.e., same X_{OA}) and at the same temperature to contain C22 in the R phase in some cases and in the T phase in others? Because the R phase is metastable with respect to the T phase, the R → T transition is highly stochastic in nature with a wide range of transition temperatures. For example, Sirota and Herhold observed this transition to occur for *n*-eicosane, C20, over a range of temperatures from 30.5 to 35.5 °C.[5] Consequently, it is possible for some particles to have already undergone this transition before they enter the flow tube and, thus, to exist in the T phase, while others are still in the R phase. Because the transition is a nonequilibrium process, it is difficult to determine exactly what governs the distribution of phases in these particles. Perhaps the aerosol consists of particles that formed with different cooling rates or with a variety of trace impurities.

What causes the increase in the fraction of particles in the T phase as the C22 content increases (i.e., as X_{OA} decreases)? Particles containing more C22 must be supercooled by larger amounts in order for the C22 to remain in the (metastable) R phase. Correspondingly, the rate of the R → T transition increases when the particles are supercooled more, so the fraction of particles remaining in the R phase decreases. In region II, the amount by which the particles are supercooled increases by only ~7 °C from $X_{OA} = 0.72$ to $X_{OA} = 0$. However, such a shift could be enough to increase significantly the rate at which the R → T transition takes place. Such a dramatic dependence on the amount of supercooling was recently observed by Weidinger et al. for the nucleation of *n*-pentadecane (C15) and *n*-heptadecane (C17) particles held in an electrodynamic balance.[18] By monitoring the intensity of polarized light scattered by the particles, they were able to measure an increase in the nucleation rates by more than an order of magnitude when the amount of supercooling increased from 9.15 to 9.8 °C for *n*-pentadecane and from 8.8 to 9.55 °C for *n*-heptadecane. Thus, it seems reasonable to expect the nucleation rate for the R → T transition also to be a strong function of the amount of supercooling, and thus composition, in the OA/C22 particles in region II. This transition might be complete for particles with $X_{OA} \leq 0.40$, as none of those decays indicates any trapping, although it was not possible to follow these reactions to completion on the time scale accessible in the flow tube experiments. Furthermore, precooling the particles with $X_{OA} = 0.40$ to 0 °C before reaction does not change the initial rate of reaction or the shape of the decay (not shown), consistent with none of the C22 existing in the R phase.

Conclusion

We have used the reaction between O_3 and OA in mixed OA/C22 particles to probe their phases and morphologies. *n*-Docosane is found to remain a supercooled liquid as much as 14 °C below the melting point and to form the metastable R solid when a sufficient fraction of the OA has reacted with O_3. This reaction-induced L → R transition completely stops the reaction by trapping the OA. When the R → T transition occurs, either when the particles are precooled or when they contain a sufficient fraction of C22 that the R solid is not stable, the reaction is seen to proceed with no trapping. The difference in reactivity between the R and T phases is attributed to the cracking of the C22 surface that occurs because of the density increase accompanying the R → T transition. Thus, the fact that the crystallization of C22 is mediated by the metastable R phase has a profound impact on particle morphology and reactivity.

Although organic aerosols in the atmosphere are much more complicated than the model binary mixture used in this study, the rates of their chemical transformation might similarly be determined by the phase and/or morphology. The results from the present work on the reaction of O_3 with an unsaturated organic species provide a starting point for understanding these effects. However, ambient aerosol contains both saturated and unsaturated organics that can react with other oxidants, including OH, and these reactions might be influenced differently. Furthermore, the particles will contain inorganic species and water, which will also affect phase and morphology, and the entropy of mixing in particles containing many different species will tend to keep them as liquids or amorphous solids.[59] Thus,

it is clear that the specific findings of the present study cannot be extrapolated directly to ambient particles. Nonetheless, it seems reasonable to expect that these particles might have much in common with the model particles used here; in particular, the rates of reactions might be influenced as much by the way in which they form as by their composition. Furthermore, intermediate or transient states could dramatically change the morphology, as demonstrated here with the C22 R → T transition. Finally, because mixtures of molecules with different chain lengths exhibit extended ranges of stability for the rotator phases, believed to be brought about by a reduction in interlayer interactions,[2,60] it is possible that the phase and/or morphology of ambient aerosols, which contain hydrocarbons of varying chain length, might be mediated by the rotator phases.

A variety of additional experiments might shed more light on the role of long-chain molecules in determining the reactivity of aerosols. For example, mixtures of *n*-alkanes with similar chain lengths ($\Delta n < 3$) could be employed to see if the increased stability of the rotator phases affects rates of reaction in the particles. Furthermore, multicomponent mixtures with a wide range of chain lengths, more closely resembling crude oil waxes, could be studied as these form orthorhombic crystalline solids[22,24] and might affect reactivity differently. Also, a systematic study with particles of different sizes might be interesting as confinement effects within particles smaller than approximately 250 nm have been observed to eliminate the rotator phase and cause the (*n*-even) *n*-alkane to adopt the orthorhombic symmetry.[46] Additionally, experiments with a variety of chain lengths might provide some insight into the role that surface freezing plays as it is known to occur only for *n*-alkanes with $14 < n \leq 50$.[15] Clearly there is much more work to be done to elucidate the complex phase behavior of these relatively simple molecules and how they influence the morphology and reactivity of organic aerosol particles.

Acknowledgment. This material is based on work supported by the National Science Foundation under Grants ATM-0402226 and ATM-0547011, as well as by the National Atmospheric and Space Administration under Grant NNX06AE86G. We also thank John Washington at the U.S. EPA National Exposure Research Laboratory in Athens, GA, for allowing us to use the differential scanning calorimeter for the bulk-phase transition studies.

References and Notes

(1) Small, D. M. *The Physical Chemistry of Lipids: From Alkanes to Phospholipids*; Plenum Press: New York, 1986; Vol. 4.
(2) Sirota, E. B.; King, H. E.; Shao, H. H.; Singer, D. M. *J. Phys. Chem.* **1995**, *99*, 798.
(3) Sirota, E. B.; King, H. E.; Singer, D. M.; Shao, H. H. *J. Chem. Phys.* **1993**, *98*, 5809.
(4) Sirota, E. B.; Herhold, A. B. *Science* **1999**, *283*, 529.
(5) Sirota, E. B.; Herhold, A. B. *Polymer* **2000**, *41*, 8781.
(6) Uhlmann, D. R.; Kritchevsky, G.; Straff, R.; Scherer, G. *J. Chem. Phys.* **1975**, *62*, 4896.
(7) Oliver, M. J.; Calvert, P. D. *J. Cryst. Growth* **1975**, *30*, 343.
(8) Earnshaw, J. C.; Hughes, C. J. *Phys. Rev. A* **1992**, *46*, R4494.
(9) Wu, X. Z.; Sirota, E. B.; Sinha, S. K.; Ocko, B. M.; Deutsch, M. *Phys. Rev. Lett.* **1993**, *70*, 958.
(10) Sefler, G. A.; Du, Q.; Miranda, P. B.; Shen, Y. R. *Chem. Phys. Lett.* **1995**, *235*, 347.
(11) Wu, X. Z.; Ocko, B. M.; Sirota, E. B.; Sinha, S. K.; Deutsch, M.; Cao, B. H.; Kim, M. W. *Science* **1993**, *261*, 1018.
(12) Shinohara, Y.; Kawasaki, N.; Ueno, S.; Kobayashi, I.; Nakajima, M.; Amemiya, Y. *Phys. Rev. Lett.* **2005**, *94*, 097801.
(13) Hughes, C. J.; Earnshaw, J. C. *Phys. Rev. E* **1993**, *47*, 3485.
(14) Wang, S. L.; Tozaki, K. I.; Hayashi, H.; Inaba, H.; Yamamoto, H. *Thermochim. Acta* **2006**, *448*, 73.
(15) Ocko, B. M.; Wu, X. Z.; Sirota, E. B.; Sinha, S. K.; Gang, O.; Deutsch, M. *Phys. Rev. E* **1997**, *55*, 3164.
(16) Sirota, E. B. *Langmuir* **1998**, *14*, 3133.
(17) Sloutskin, E.; Sirota, E. B.; Kraack, H.; Ocko, B. M.; Deutsch, M. *Phys. Rev. E* **2001**, *64*, 031708.
(18) Weidinger, I.; Klein, J.; Stockel, P.; Baumgartel, H.; Leisner, T. *J. Phys. Chem. B* **2003**, *107*, 3636.
(19) Ofer, E.; Sloutskin, E.; Tamam, L.; Ocko, B. M.; Deutsch, M. *Phys. Rev. E* **2006**, *74*.
(20) Nakasone, K.; Shiokawa, K.; Urabe, Y.; Nemoto, N. *J. Phys. Chem. B* **2000**, *104*, 7483.
(21) Povey, M. J. W.; Hindle, S. A.; Aarflot, A.; Hoiland, H. *Cryst. Growth Des.* **2006**, *6*, 297.
(22) Srivastava, S. P.; Handoo, J.; Agrawal, K. M.; Joshi, G. C. *J. Phys. Chem. Solids* **1993**, *54*, 639.
(23) Srivastava, S. P.; Saxena, A. K.; Tandon, R. S.; Shekher, V. *Fuel* **1997**, *76*, 625.
(24) Dirand, M.; Chevallier, V.; Provost, E.; Bouroukba, M.; Petitjean, D. *Fuel* **1998**, *77*, 1253.
(25) Jacobson, M. C.; Hansson, H. C.; Noone, K. J.; Charlson, R. J. *Rev. Geophys.* **2000**, *38*, 267.
(26) Hildemann, L. M.; Rogge, W. F.; Cass, G. R.; Mazurek, M. A.; Simoneit, B. R. T. *J. Geophys. Res.-Atmos.* **1996**, *101*, 19541.
(27) Schauer, J. J.; Kleeman, M. J.; Cass, G. R.; Simoneit, B. R. T. *Environ. Sci. Technol.* **1999**, *33*, 1578.
(28) Tobias, H. J.; Beving, D. E.; Ziemann, P. J.; Sakurai, H.; Zuk, M.; McMurry, P. H.; Zarling, D.; Waytulonis, R.; Kittelson, D. B. *Environ. Sci. Technol.* **2001**, *35*, 2233.
(29) Morris, J. W.; Davidovits, P.; Jayne, J. T.; Jimenez, J. L.; Shi, Q.; Kolb, C. E.; Worsnop, D. R.; Barney, W. S.; Cass, G. *Geophys. Res. Lett.* **2002**, *29*, L014692.
(30) Moise, T.; Rudich, Y. *J. Phys. Chem. A* **2002**, *106*, 6469.
(31) Smith, G. D.; Woods, E.; III; DeForest, C. L.; Baer, T.; Miller, R. E. *J. Phys. Chem. A* **2002**, *106*, 8085.
(32) Asad, A.; Mmereki, B. T.; Donaldson, D. J. *Atmos. Chem. Phys. Discuss.* **2004**, *4*, 4019.
(33) Hearn, J. D.; Smith, G. D. *J. Phys. Chem. A* **2004**, *108*, 10019.
(34) Katrib, Y.; Martin, S. T.; Hung, H.-M.; Rudich, Y.; Zhang, H.; Slowik, J. G.; Davidovits, P.; Jayne, J. T.; Worsnop, D. R. *J. Phys. Chem. A* **2004**, *108*, 6686.
(35) King, M. D.; Thompson, K. C.; Ward, A. D. *J. Am. Chem. Soc.* **2004**, *126*, 16710.
(36) LaFranchi, B. W.; Zahardis, J.; Petrucci, G. A. *Rapid Commun. Mass Spectrom.* **2004**, *18*, 2517.
(37) Thornberry, T. D.; Abbatt, J. P. D. *Phys. Chem. Chem. Phys.* **2004**, *6*, 84.
(38) Hearn, J. D.; Lovett, A. J.; Smith, G. D. *Phys. Chem. Chem. Phys.* **2005**, *7*, 501.
(39) Zahardis, J.; Petrucci, G. A. *Atmos. Chem. Phys.* **2007**, *7*, 1237.
(40) Hearn, J. D.; Smith, G. D. *Phys. Chem. Chem. Phys.* **2005**, *7*, 2549.
(41) Knopf, D. A.; Anthony, L. M.; Bertram, A. K. *J. Phys. Chem. A* **2005**, *109*, 5579.
(42) Ziemann, P. J. *Faraday Discuss.* **2005**, *130*, 469.
(43) Nash, D. G.; Tolocka, M. P.; Baer, T. *Phys. Chem. Chem. Phys.* **2006**, *8*, 4468.
(44) Hearn, J. D.; Smith, G. D. *Int. J. Mass Spectrom.* **2006**, *258*, 95.
(45) Wang, S. L.; Tozaki, K.; Hayashi, H.; Hosaka, S.; Inaba, H. *Thermochim. Acta* **2003**, *408*, 31.
(46) Montenegro, R.; Landfester, K. *Langmuir* **2003**, *19*, 5996.
(47) Sirota, E. B.; Singer, D. M. *J. Chem. Phys.* **1994**, *101*, 10873.
(48) Brambilla, L.; Zerbi, G. *Macromolecules* **2005**, *38*, 3327.
(49) Taggart, A. M.; Voogt, F.; Clydesdale, G.; Roberts, K. J. *Langmuir* **1996**, *12*, 5722.
(50) Sirota, E. B. *J. Chem. Phys.* **2000**, *112*, 492.
(51) Li, H. Z.; Yamamoto, T. *J. Chem. Phys.* **2001**, *114*, 5774.
(52) Li, H. Z.; Yamamoto, T. *J. Phys. Soc. Jpn.* **2002**, *71*, 1083.
(53) Zhang, Y.; Ou-Yang, Z. C.; Iwamoto, M. *J. Chem. Phys.* **2006**, *124*, 214906.
(54) Xie, B. Q.; Shi, H. F.; Jiang, S. C.; Zhao, Y.; Han, C. C.; Xu, D. F.; Wang, D. J. *J. Phys. Chem. B* **2006**, *110*, 14279.
(55) Vieceli, J.; Ma, O. L.; Tobias, D. J. *J. Phys. Chem. A* **2004**, *108*, 5806.
(56) Snyder, R. G.; Maroncelli, M.; Qi, S. P.; Strauss, H. L. *Science* **1981**, *214*, 188.
(57) Templin, P. R. *Ind. Eng. Chem.* **1956**, *48*, 154.
(58) Sirota, E. B. *Macromolecules* **2007**, *40*, 1043.
(59) Marcolli, C.; Luo, B. P.; Peter, T. *J. Phys. Chem. A* **2004**, *108*, 2216.
(60) Herhold, A. B.; King, H. E.; Sirota, E. B. *J. Chem. Phys.* **2002**, *116*, 9036.